

Journal Pre-proof

Probing fouling mechanism of anion exchange membranes used in electro dialysis self-reversible treatment by humic acid and calcium ions



M.A.C.K. Hansima , J. Ketharani , D.R. Samarajeewa ,
K.G.N. Nanayakkara , Ajith C. Herath ,
Madhubhashini Makehelwala , Suresh Indika , K.B.S.N. Jinadasa ,
S.K. Weragoda , Yuansong Wei , Rohan Weerasooriya

PII: S2666-8211(21)00089-2
DOI: <https://doi.org/10.1016/j.ceja.2021.100173>
Reference: CEJA 100173

To appear in: *Chemical Engineering Journal Advances*

Received date: 27 May 2021
Revised date: 1 August 2021
Accepted date: 21 August 2021

Please cite this article as: M.A.C.K. Hansima , J. Ketharani , D.R. Samarajeewa , K.G.N. Nanayakkara , Ajith C. Herath , Madhubhashini Makehelwala , Suresh Indika , K.B.S.N. Jinadasa , S.K. Weragoda , Yuansong Wei , Rohan Weerasooriya , Probing fouling mechanism of anion exchange membranes used in electro dialysis self-reversible treatment by humic acid and calcium ions, *Chemical Engineering Journal Advances* (2021), doi: <https://doi.org/10.1016/j.ceja.2021.100173>

This is a PDF file of an article that has undergone enhancements after acceptance, such as the addition of a cover page and metadata, and formatting for readability, but it is not yet the definitive version of record. This version will undergo additional copyediting, typesetting and review before it is published in its final form, but we are providing this version to give early visibility of the article. Please note that, during the production process, errors may be discovered which could affect the content, and all legal disclaimers that apply to the journal pertain.

© 2021 Published by Elsevier B.V.
This is an open access article under the CC BY-NC-ND license
(<http://creativecommons.org/licenses/by-nc-nd/4.0/>)

Probing fouling mechanism of anion exchange membranes used in electro dialysis self-reversible treatment by humic acid and calcium ions

M. A. C. K. Hansima^a, J. Ketharani^b, D. R. Samarajeewa^b, K. G. N. Nanayakkara^b, Ajith C. Herath^c
Madhubhashini Makehelwala^{d,*}, Suresh Indika^f, K. B. S. N. Jinadasa^b, S. K. Weragoda^{d,e}, Yuansong
Wei^{f,g}, Rohan Weerasooriya^{d,g,*}

^a Post Graduate Institute of Science (PGIS), University of Peradeniya, Sri Lanka.

^b Department of Civil Engineering, Faculty of Engineering, University of Peradeniya, Sri Lanka.

^c Department of Chemical Sciences, Faculty of Applied Sciences, Rajarata University of Sri Lanka.

^d China Sri Lanka Joint Research and Demonstration Centre for Water Technology, Ministry of Water Supply, Prof E.O.E Pereira Mawatha, Meewathura, Peradeniya 20400, Sri Lanka.

^e National Water Supply and Drainage Board, Katugastota 20800, Sri Lanka.

^f Department of Water Pollution Control Technology, Research Centre for Eco-Environmental Sciences, Chinese Academy of Sciences, Beijing 100085, China.

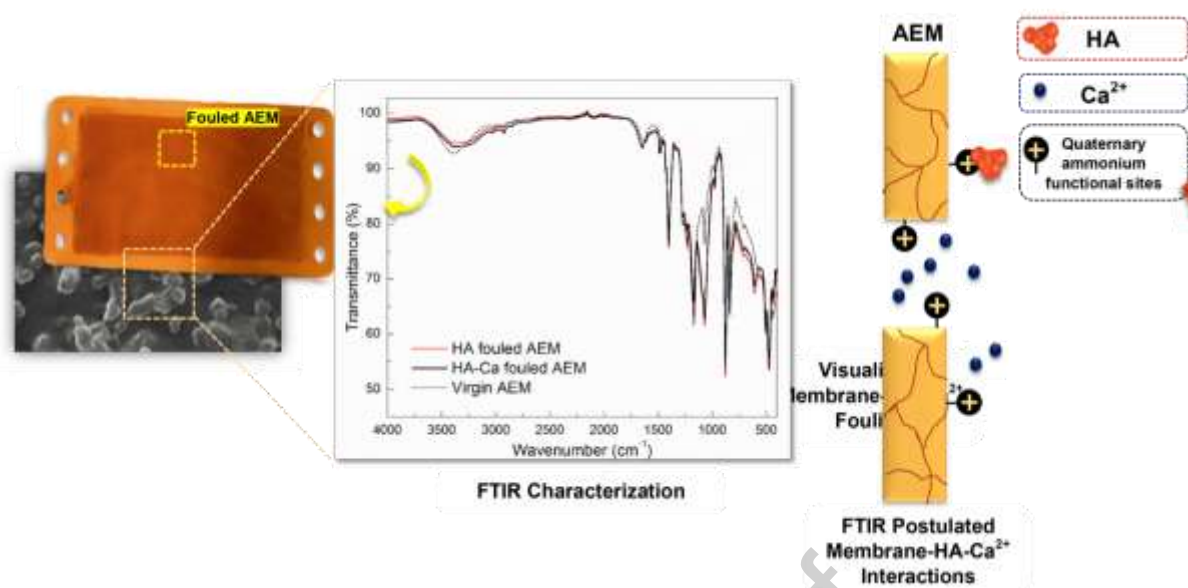
^g National Center for Water Quality Research, National Institute of Fundamental Studies, Kandy 20000, Sri Lanka.

*Corresponding authors: China Sri Lanka Joint Research and Demonstration Centre for water technology, Ministry of Water Supply, Prof E.O.E. Pereira Mawatha, Meewathura, Peradeniya 20400, Sri Lanka; Email Address: depdirec_rt.jrdc@mws.gov.lk; rohan.we@nifs.ac.lk

Highlights

- Self-reversal in EDR and chemical desorption fail to remove humic foulants
- Predominant forces of HA fouling are electrostatic forces
- Major forces of HA-Ca²⁺ fouling are hydrophobic forces
- Incorporation of Ca²⁺ ions enhances irreversibility of the HA-Ca²⁺ fouling

Graphical Abstract



Abstract

When humic substances (HS) are present in the feed water, fouling of ion-exchange membranes is inevitable despite the built-in self-cleaning process of electro dialysis reversal systems (EDR). When Ca^{2+} is present in water, HS can readily chelate with them and form organic- Ca^{2+} complexes, which can foul anion exchange membranes (AEMs) in an irreversible manner. However, the elucidation of distinct processes between membrane scaling by Ca^{2+} and fouling by HS- Ca^{2+} complexes is debated. We examined the AEM fouling by Ca^{2+} and HS using synthetic groundwater. Well-characterized Sigma-Aldrich humic acid (HA) was used to adjust the dissolved organic carbon content in the water. Forcefully fouled AEM by HA and HA- Ca^{2+} was treated with 2% (w/w) NaCl and 0.03% (w/w) sodium dodecyl sulfate to destabilize the organic moieties on the membranes. The bonding types of HA- Ca^{2+} and HA with the membrane were examined by vibrational spectroscopy. The surface topographies were visualized by scanning electron microscopy. Both inter- and intramolecular interactions, including hydrophobic cation- π interactions among HA- Ca^{2+} complexes, were active in membrane fouling. Size compatibility and reduced surface charge of HA- Ca^{2+} (compared to HA) seems to alter the AEM self-cleaning process leading to irreversible fouling. Based on the vibrational spectral evidence, a plausible AEM fouling mechanism by HA- Ca^{2+} is proposed. Identification of interactions between the membrane and the foulant will provide an insight into designing appropriate self-cleaning protocols in EDR.

Keywords: EDR, anion exchange membrane, membrane fouling interactions, humic substances, calcium ion, ternary complexes

1. Introduction

Dissolved organic matter (DOM), consisting of humic substances (HS), polysaccharides, proteins etc., is ubiquitous in natural waters. Its concentration typically ranges between 0.1 to 10 mg L⁻¹ [1, 2]. HS is operationally classified as a) humins (MW: 100-10 000 kDa, acid-base insoluble fraction), b) humic acids (HA) (MW: 10-100 kDa, acid-insoluble and base soluble fraction), and c) fulvic acids (FA) (MW: 1-10 kDa, acid and base soluble fraction) [3]. HS possess heterogeneous cross-polymeric arrays of aromatic, cyclic and aliphatic organic structures formed during humification [3, 4]. The aliphatic and aromatic carboxyl (-COOH), hydroxyl (-OH), alkoxy (R-O-R,-O-R) as well as aliphatic carbonyl (-CO-) groups are most common in FA and HA fractions [5, 6]. Chelation of DOM and metal ions occurs at carboxylic and phenolic groups via inner or outer-sphere complexation. Physico-chemical properties of DOM moieties seem to change upon metal ion complexation [7]. Hence, particular attention should be paid to elucidate the mechanisms of metal ions-DOM interactions in designing effective water treatment technologies, e.g., coagulation, flocculation, membrane separation [7, 8, 9].

Ion exchange membranes (IEMs) used in electrodialysis reversal (EDR) systems, viz. anion exchange membranes (AEMs) and cation exchange membranes (CEMs), enrich anions and cations into separate compartments. The negatively charged HS permeates through AEMs. EDR technology uses a self-reversal process to clean membrane surfaces periodically. However, HS can foul membranes, irrespective of the EDR self-cleaning cycle, and the exact fouling mechanism has not been resolved yet [10]. HS can also trigger other geochemical processes like precipitation, aggregation, complexation, etc., enhancing membrane fouling. The membrane fouling by HS mainly depends on hydrophobicity, functional groups, surface roughness, nano-channelling, solution pH, macromolecular structure, and molecular weight of HS fractions [8, 9]. Membrane fouling typically occurs via inter-and intramolecular bonding and the foulant-foulant interactions also intensify the degree of membrane fouling [12, 13].

Both HS and inorganic colloids possess pH-dependent charge sites, and they interact with the membranes forming electrostatic (reversible fouling) or chemical bonds (irreversible fouling).

IEM fouling by amino acids [11], tannins [14], sulfonated resins [15], or sodium dodecylbenzene sulfonate [16] has been extensively examined considering electrostatic attractions between foulants and the membrane sites. The reversibly fouled membranes can be restored using cleaning cycles with appropriate cleaning agents [10]. However, dissolved HS (e.g., humic acids and fulvic acids) can form ternary complexes with metal ions and membrane surface sites (e.g., membrane-HS-M^{2+/3+}), leading to irreversible fouling. Both inter and intramolecular interactions play a pivotal role in the membranes' irreversible fouling [17]. To the best of our knowledge, research into an in-depth investigation of the IEM fouling mechanisms by HS-M^{2+/3+}-membrane ternary complexes, especially due to Ca²⁺ or other abundant cations (M^{2+/3+}) in water, is scarce.

Ca²⁺ is ubiquitous in hard water, which can deactivate the membranes by scaling. However, in the presence of organic chelates, irreversible fouling may occur with an inconclusive mechanism. In this work, we examined the membrane fouling mechanisms by HA-Ca²⁺ complexes using synthetic water. Well-characterized Sigma-Aldrich humic acid was used to represent the DOM in the water. The fouling mechanism of the AEMs by ternary complexes was resolved by Attenuated Total Reflectance Fourier Transform Infrared (ATR-FTIR) spectroscopy and Scanning Electron Microscopy-Energy Dispersive X-Ray Spectroscopy (SEM-EDX). Vibrational spectral signatures of HA-fouled and HA-Ca²⁺-fouled membranes were used to identify the impact of Ca²⁺ in HS-M^{2+/3+}-membrane complex formation.

Salt solutions are capable of detaching foulants interacted electrostatically with membranes by destabilizing them. For example, Persico et al. (2017a, b) used NaCl as a desorption solution to remove peptide fouling from CEMs. They explained that, positively charged peptides interacted electrostatically with negative sulfonate sites of CEMs can be desorbed with NaCl [11,18]. Similarly, sodium dodecyl sulfonate (SDS) is used as a desorption reagent to desorb hydrophobically adsorbed substances from a surface [19]. In this study, a sequential desorption was also carried out for fouled membranes, first by a 2.0% (w/w) NaCl solution and then by a 0.03% (w/w) SDS solution, to reveal the recovery of the membranes. The extensive investigation of the IEM fouling interactions by HA in the presence of Ca²⁺ suggested seeking for appropriate pretreatment methods to exempt DOC-Ca²⁺ present in groundwater to enhance membrane durability of the EDR systems.

Materials and Methods

2.1 Ion exchange membranes

CJMA-4 (anion exchange) and CJMC-4 (cations exchange) IEMs were purchased from Hefei ChemJoy Polymer Materials Co. (China). The membranes were built on polyvinylidene fluoride (PVDF) matrix with quaternary ammonium ($-N^+(CH_3)_3$) or sulfonate ($-SO_3^-$) groups for the AEMs, or CEMs fabrication. The AEM characterization data are summarized in **Table S.1** (Table 1 support documentation). According to the specifications given by the manufacturer, new membranes were soaked in distilled water for conditioning.

2.2 Chemicals

Unless otherwise specified, analytical grade chemicals were purchased from Sigma-Aldrich (USA). Potassium hydrogen phthalate was used to calibrate the Total Organic Carbon (TOC) analyzer for DOC measurements. $\sim 2 \text{ mg L}^{-1}$ HA and HA- Ca^{2+} solutions were prepared using Sigma-Aldrich humic acid. Distilled water was used in all experiments (JP Selecta AC-L4, Greece). The chemical and physical properties of well-characterized Sigma-Aldrich humic acid are summarized in **Table S.2**.

2.3 Fouling experiments

Preparation of the feed solutions: The feed solutions were prepared to mimic groundwater conditions as detailed elsewhere [20]. A 1 L of $\sim 2 \text{ mg L}^{-1}$, TOC HA feed solution was prepared by mixing $0.0056 (\pm 0.0001)$ g of Sigma-Aldrich humic acid in 0.001 M NaCl and 0.001 M $NaHCO_3$. A 1 L of $\sim 2 \text{ mg L}^{-1}$, TOC HA- Ca^{2+} feed solution was prepared by mixing $0.0098 (\pm 0.0001)$ g Sigma-Aldrich humic acid and 200 mg L^{-1} $CaCl_2 \cdot 2H_2O$ in 0.001 M NaCl and 0.001 M $NaHCO_3$. Both solutions were stirred for 24 hours using a magnetic heating stirrer at 550 rpm speed at 22°C and pH 11.44. The resultant solutions were filtered through PES membrane filters ($0.45 \mu\text{m}$) to yield dissolved HS fractions. The initial pH of the feed solutions was adjusted to 8 with the 1 M HCl.

EDR setup: The EDR membrane stack system was purchased from Hefei ChemJoy Polymer Materials Co. (China). **Fig. S.1** (Figure 1 support documentation) shows the stack assembly, and **Table S.3** shows the specifications. A regulated DC power supply (LODESTAR; LP300SD) was used to apply the required potential across the EDR cell. The pH (pH probe; Orion 910003, U.S.A) and conductivity (conductivity cell probe; Orion 013010MD, U.S.A) in dilute and concentrate chambers were monitored with time using a multiparameter meter

(Thermo Orion A325, USA). The TDS of the solutions were calculated using built-in functions in the multiparameter. The pH of the dilute and the concentrate chambers was adjusted to ~8 with 1 M NaOH or 1 M HCl. Dilute, concentrate, and the electrode rinse solutions (ERS) was pumped to the EDR system using a 4-way variable speed peristaltic pump (Lead fluid; WT600S) at 0.3 L min⁻¹ flow rate. The initial volume for all three input solutions was applied as 400 mL in each batch. Before starting an experiment, each chamber was circulated with new solutions for around 5 min to eliminate air bubbles from the system. For a typical fouling experiment, the treatment time was ~40 min at ambient temperature.

Analytical methods: The DOC content of the samples was measured by TOC analyzer (Shimadzu TOC-L CSH/CSN, Japan), Ultraviolet absorbance at λ 254 nm was measured using Ultraviolet-Visible (UV-Vis) spectrophotometer (Shimadzu UV-2700), and the calcium ion concentrations were measured by flame Atomic Absorption Spectrophotometer (Shimadzu AA-7000, Japan). The desalination efficiency (D, %) of the feed solutions of each batch was calculated using **equation 1** [21], where σ_0 and σ_t are electrical conductivity (mS cm⁻¹) at $t = 0$ and t respectively in the dilute compartment.

$$D = \frac{\sigma_0 - \sigma_t}{\sigma_0} \times 100\% \quad (1)$$

The decolourisation efficiency (A, %) of the feed solutions in each batch was calculated by **equation 2** [22], where A_0 and A_t are initial and final UV₂₅₄ absorbance values of the feed solution at $t = 0$ and after time t , respectively.

$$A = \frac{A_0 - A_t}{A_0} \times 100\% \quad (2)$$

Removal rate (R, %) of HS from the dilute compartment during the treatment of each batch was calculated according to **equation 3** [23], using the initial DOC concentration (C_0 in mg L⁻¹) and the final DOC concentration (C_t in mg L⁻¹). The calcium ion removal rate was calculated using the initial and final Ca²⁺ concentrations (mg L⁻¹) for the HA-Ca²⁺ feed solution.

$$R = \frac{C_t}{C_0} \times 100\% \quad (3)$$

2.4 Desorption experiments

The AEM was disassembled from the EDR system and dried in a desiccator (**Fig. S.2 (a)** and **(b)**). The fouled membrane was cut into small pieces (0.5 cm × 0.5 cm). Sequential

desorption was carried out by soaking membranes in 100 mL 2.0% (w/w) NaCl for 24 h while stirring; then, the membrane pieces were soaked 100 mL of 0.03% (w/w) SDS solution for 24 h while stirring. EC, pH, DOC and Ca^{2+} concentrations of desorption solutions were determined. Fouled and desorbed membranes were then analyzed using SEM-EDX (EVO 18; ZEISS, Germany) and ATR-FTIR (UATR two; PerkinElmer, USA).

3. Results and discussion

3.1 Fouling experiments

The initial current flux of the EDR is governed by the concentration gradient of ions in the interfacial region of the feed side. The direction of ions' migration is determined by the potential gradient applied across the EDR stack. Current flux in the feed solution is enhanced in the presence of monovalent ions (Na^+ , Cl^- , HCO_3^-) and divalent (Ca^{2+}) ions with high mobility. These ions are more mobile and selective than other charged species in the solution [19, 20]. Hence, the effect of HS on the current flux of the EDR is minimal. However, the deposition of HS lowers the movement of the mobile ions across the AEM, thereby reduces the current flux. As shown in **Fig. 1 (a-b)**, the degree of AEM fouling by HA or HA- Ca^{2+} was determined by the conductivity measurements of permeates. Within a batch cycle, the conductivity of the permeate has decreased. The spikes observed during each polarity reversal phase were due to the mixing of the permeate and the concentrate at off-specification periods as the solution carried over from the previous cycle introduces extra conductivity to the next batch.

Fig. 1

The solutes/ ions concentration near the membrane surface has decreased with time; hence the current flux is reduced, creating an ion deficit interface. At extreme ion deficit conditions water splitting occurs on the IEM surface generating H^+ and OH^- which results in an enhanced current flux [21, 22]. The water splitting is enhanced significantly on the surface of HS fouled membranes [27, 28]. As a result, the solution pH in the dilute compartment decreases while showing an opposite trend in pH variations in the concentrate compartment. Therefore, the feed water requires pH adjustments to nullify HA protonation or deprotonation.

When HA was used in the feed solution, the inlet pipe between the AEM and spacer has blocked due to fouling after the fourth cycle in the batch mode experiment. This was readily

visible when the EDR stack was dismantled (**Fig. S.2**). However, when HA-Ca²⁺ was used in the feed solution, fouling at the above location (**Fig. S.2**) was delayed till the seventh cycle. Hence it is arguable that, when HA is present in the feed, the AEM fouling occurs more rapidly than HA-Ca²⁺ feed solution. AEM fouling is promoted by the negative charge of the HA [29, 30]. However, when HA-Ca²⁺ is present, the negative charge density of the organic moiety is reduced due to the complexation of metal ions [7, 25, 26, 33], delaying membrane fouling.

Fig. 2 (a) and **(b)** show the decline of desalination and decolourization removal efficiencies in permeate water when HA and HA-Ca²⁺ are used in the feed solution due to AEM membrane fouling. Further, the reduction of the negative charge of HA in HA-Ca²⁺ resulted in lower DOC removal rates by the EDR membranes (<50%) in comparison to HA (>90%). The surface titrations of HA and HA-Ca²⁺ solutions in 0.1 M NaCl showed that the negative charge of the organic moieties has reduced when Ca²⁺ is present (Supplementary data). When HA-Ca²⁺ is present in the feed solution, the Ca²⁺ removal rate by the AEM was increased from batch 1 to batch 7 (**Fig. 2 (b)**). The Ca²⁺ in the feed solution can remove in several ways; in one way, Ca²⁺ can be removed by CEM; alternatively, HA can form HA-Ca²⁺ complexes that AEM can remove. Thus, free Ca²⁺ facilitates the bridging of HA onto membrane sites, providing preferred alignments for hydrophobic bonding between the HA moieties and the membrane surface. Further, Ca²⁺ attached membrane sites can serve as nucleation sites to form inorganic scalants like Ca(OH)₂.

Fig. 2

	2% (w/w) NaCl solution				0.03% (w/w) SDS solution			
	pH	DOC (mg/L)	Ca ²⁺ (mg/L)	EC (mS/cm)	pH	DOC (mg/L)	Ca ²⁺ (mg/L)	EC (μ S/cm)
Initial	6.24 \pm 0.13	0.00 \pm 0.00	-	18.21 \pm 0.89	3.88 \pm 0.03	70.21 \pm 15.91	-	104.57 \pm 13.55
Final (HA)	5.76 \pm 0.33	0.19 \pm 0.30	-	18.18 \pm 0.91	3.87 \pm 0.05	0.08 \pm 0.14	-	207.83 \pm 15.65
Final (HA-Ca ²⁺)	6.05 \pm 0.06	0.64 \pm 0.33	0.08 \pm 0.04	18.14 \pm 0.85	3.86 \pm 0.03	0.33 \pm 0.47	-	217.80 \pm 41.29
Final (Virgin)	7.08 \pm 0.03	0.00 \pm 0.00	-	18.23 \pm 1.02	3.86 \pm 0.06	0.00 \pm 0.00	-	214.6 \pm 10.53

Table 1: Solution properties of 2% (w/w) NaCl and 0.03% (w/w) SDS desorption solutions at RT before and after the equilibration with fouled AEMs

3.2 Desorption study

EDR self-reversal process and the chemical washing are ineffective for irreversible membrane fouling. The fraction of irreversible foulants on AEMs can be determined by sequential desorption experiments. The cleaning of the fouled membrane was carried out with 2% (w/w) NaCl and 0.03% (w/w) SDS, and the solution properties of the desorbed solutions are shown in **Table 1**. When the virgin membranes were desorbed with 2% (w/w) NaCl, the increased solution pH was ascribed to OH⁻ and Cl⁻ exchange. However, when the fouled membranes by HA or HA-Ca²⁺ were desorbed, the solution pH was decreased by detaching protonated HS from the membrane.

Further, the desorbed HA had a higher quantity of protons (-COOH, pH 5.76) compared to HA-Ca²⁺ (pH 6.05) indicating Ca²⁺ complexation (-COO⁻-Ca²⁺ in carboxyl sites). The NaCl treated HA-Ca²⁺ fouled membrane contained high DOC content due to high fouling intensity. Ca(OH)₂ scalants were readily visible in the membranes treated with HA-Ca²⁺ feed solution (**Fig. S.3**). The density of the scalants diminished upon the NaCl treatment due to Ca(OH)₂ dissolution. Enhanced membrane scaling in the presence of HS in the feed solution is reported previously [34]. SDS is a well-known cleaning agent used to destabilize hydrophobic foulants [11]. The pH of the solution after SDS treatment did not vary significantly; however, the EC was increased. Importantly, as can be depicted by data the amount of HS-Ca²⁺ removal by SDS was high, indicating enhanced hydrophobicity of the foulants by cation- π bridging interactions. The IR data suggested that the foulants could be diminished from the membrane surfaces to some extent by cleaning agents. Still, the

membrane functionality cannot be restored (section 3.3). The increased EC values of the NaCl and SDS solutions treated by virgin membrane were not due to carbon-derived materials. The SDS adsorption on the virgin AEM has decreased the solution DOC content from 70.21 to 0.00 mg L⁻¹. Increased EC after the SDS desorption is due to the desorption of HA and complexed Ca²⁺ ions.

3.3 Characterization of the fouled and desorbed membranes

Fig. 3

SEM-EDX analysis: SEM images and EDX elemental data of virgin, fouled and desorbed AEMs are used to identify the surface morphology of fouled membranes after chemical cleaning. As shown in **Fig. 3 (a)**, the pores of the virgin AEM membrane have widened upon the NaCl treatment thus facilitating the ion exchange. The elemental composition of the NaCl treated virgin membrane shows surface-bound Cl. Compared to virgin membrane, the NaCl treated membranes, the O% was decreased by 2.05%, and Cl% was increased by 2.71%, indicating the substitution of Cl⁻ to OH⁻ (**Table S.4**). As observed in **Fig. 3 (b)** and **(c)**, both foulants seemed to accumulate within the AEM pores. Quaternary amine functional sites are located within the pores [35]. Therefore, initiation and establishment of membrane-foulant interactions should occur within pores, which cause severe irreversible fouling with humic substances. The EDX data of the HA and HA-Ca²⁺ fouled membranes showed an increased O content compared to the virgin membrane (for HA; from virgin 2.05% to fouled 6.15% and for HA-Ca²⁺; from virgin 2.05% to fouled 6.07%). The appearance of the sulfur peak suggests the presence of HA as the foulant. As seen from the SEM images, HA-Ca²⁺ fouling covered 33.90%, and HA fouling covered 30.74% of the membrane surface. The fluoride content on HA-Ca²⁺ fouled membrane surface was reduced significantly (from 37.75% to 34.45%) than HA, indicating high coverage by HA-Ca²⁺. The intense fouling of the membrane by HA-Ca²⁺ may block the passage of the electron beam of the SEM into the membrane surface, which may be the reason for the reduced F content.

The observed surface morphologies of HA fouled AEM, and HA-Ca²⁺ fouled AEM are different (**Fig. 3 (b)** and **(c)**). The HA-Ca²⁺ foulant showed relatively large aggregations compared to that of the HA fouled membranes. The size of HA aggregates in the presence of multivalent cations and at different solution pH values were reported in the literature [30]. In

agreement with the published data, HA readily undergoes aggregation due to inter- or intramolecular bridging by Ca^{2+} [36].

As shown in **Fig. 3 (d)** and **(e)**, the NaCl solution was ineffective in removing HA derived foulants completely from the AEM due to the incomplete destabilization of surface adhered organic moieties. The NaCl treated membranes showed widened pores due to stripping of electrostatically retained foulants. The SDS desorption should remove foulants that are hydrophobically attached to the membrane [8, 31]. After the SDS treatment, the fouled membranes were not recovered markedly. Instead, we noted SDS self-fouling zones on the membrane (**Fig. 3 (f)** and **(g)**). Recent evidence shows that SDS itself can act as a foulant [32, 33, 34]. In the presence of SDS, membrane fouling by HS was not readily apparent. SDS may interact with hydrophobic regions of the membrane or with surface-bound HS after the NaCl treatment. However, SDS accumulation intensity was comparatively higher for HA- Ca^{2+} fouled AEM membranes, indicating the replacement of HA- Ca^{2+} by SDS. EDX results showed that the SDS desorbed fouled membranes have a noticeable increase in the S content as compared to the virgin membrane. This is due to the secondary fouling of partially fouled membranes by SDS. The interactions of SDS and AEMs were further characterized using ATR-FTIR.

ATR-FTIR analysis: Membrane fouling initiates via membrane and foulant interactions. The foulant-foulant interactions intensify the degree of membrane fouling [13]. We used vibrational spectroscopy data to elucidate molecular interactions between HA and HA- Ca^{2+} with the AEM. To identify membrane fouling by HA in the presence of Ca^{2+} , the fingerprint and functional groups regions of IR spectrums, and de-convoluted bands for COO^- and $^+\text{N}-\text{C}$ vibrations at $1720\text{-}1560\text{ cm}^{-1}$, and COOH vibrations at $1140\text{-}1040\text{ cm}^{-1}$ were used (**Fig. 4**). FTIR spectrums at high (ν , $4000\text{-}2500\text{ cm}^{-1}$), mid (ν , $1800\text{-}1300\text{ cm}^{-1}$) and low (ν , $1400\text{-}500\text{ cm}^{-1}$) frequency regions of 2% w/w NaCl and 0.03% w/w SDS treated HA fouled and HA- Ca^{2+} fouled membranes are shown in **Fig 5**.

Fig. 4

Fig. 5

O–H and C–H stretching vibration region ($\sim 3670\text{-}2850\text{ cm}^{-1}$): As shown in **Fig. 4 (a)**, the IR band around 3382 cm^{-1} due to H-bonded O–H stretching vibration ($\nu_{(\text{O-H})}$) has widened due to $\nu_{(\text{O-H})}$ of phenolic or carboxyl groups indicating the appearance of the HA/HA- Ca^{2+}

foulants on the AEM surface. The redshift of the O–H stretching vibration region ($\Delta\nu \sim 38 \text{ cm}^{-1}$) observed for fouled membranes by HA or HA-Ca²⁺ compared to the virgin membrane, is ascribed to the H-bonding between water and bound F in PVDF sites, and the foulants' carboxylate and phenolate groups. Similar red shifts have been reported in literature [35, 36]. The $\nu_{(\text{O-H})}$ band resulted from both the HA and HA-Ca²⁺ fouled membranes have narrowed and reduced the intensity upon NaCl and SDS treatments (**Fig. 5 (a), (b)**). The desorb solutions destabilized foulants adhered to the outer-most surface facilitating their desorption [8, 31, 37]. However, the intensity of the $\nu_{(\text{O-H})}$ band in the HA-Ca²⁺ fouled membrane only reduced with NaCl but not with SDS, showing strengthened irreversible hydrophobic interactions of inner-most fouling layers on the membrane (**Fig. 5 (b)**). The broadening of CH₂ symmetric band ($\nu_{(\text{C-H}) \text{ sym}}$) at 2960.7 cm^{-1} compared to the virgin membrane is attributed to the appearance of aromatic C–H [36, 38, 40]. The $\nu_{(\text{C-H}) \text{ sym}}$ band of HA or HA-Ca²⁺ fouled membrane has blue shifted (compared to the virgin membrane) by $\Delta\nu 14.9 \text{ cm}^{-1}$ or 11.0 cm^{-1} , respectively due to hydrophobic CH– π interactions (**Fig. 4 (a)**). The C–H stretching at 3029.8 cm^{-1} , attributed to PVDF membrane H–C–N⁺ groups showed red shifts after HA fouling by $\Delta\nu 1.3 \text{ cm}^{-1}$ and after HA-Ca²⁺ fouling by $\Delta\nu 0.7 \text{ cm}^{-1}$. These shifts are due to the electrostatic interactions between the membrane and the foulant. Therefore, the data suggested the existence of less electrostatic interactions for HA-Ca²⁺ complexes due to their comparatively less negative surface potential after Ca²⁺ chelation [44, 45]. NaCl and SDS desorption have reduced the intensities of the peaks in this region, indicating deteriorated membrane surface features while appearance of SDS features upon the desorption by the SDS solution (CH₂ at 2966 cm^{-1} ($\nu_{(\text{C-H}) \text{ sym}}$), CH₂ ($\nu_{(\text{C-H}) \text{ asym}}$) at 3023 cm^{-1} , CH₃ ($\nu_{(\text{C-H}) \text{ sym}}$) at 2851 cm^{-1} and CH₃ ($\nu_{(\text{C-H}) \text{ asym}}$) at 2923 cm^{-1}) [46] (**Fig. 5**). Intense SO₂ asymmetric IR bands ($\nu_{(\text{SO}_2) \text{ asym}}$) appeared at 1169 cm^{-1} and 1232 cm^{-1} and the symmetric band ($\nu_{(\text{SO}_2) \text{ sym}}$) at 1074 cm^{-1} confirmed the SDS-induced fouling after the foulant desorption. Vibrational data observed from the desorption study revealed that the membrane functionality cannot be restored by chemical cleaning because the foulants have destructed the membranes irreversibly. Enhanced irreversible fouling by HA-Ca²⁺ was previously hypothesized by our team to explain the failure in self-reversal mechanisms to purge the foulant from the AEM surfaces [10].

C=C stretching vibration region ($\sim 1720\text{-}1560 \text{ cm}^{-1}$): The de-convoluted peaks of the C=C stretching vibrational region shown in **Fig. 4 (c), (d), and (e)** for HA-Ca²⁺ fouling, HA fouling and virgin membrane, respectively, varied markedly. Accordingly, the broad ⁺N–C stretch ($\nu_{(+\text{N-C})}$) of quaternary amine functional sites at 1646.1 cm^{-1} and the C=C stretch

($\nu_{(C=C)}$) at 1613.61 cm^{-1} observed in the virgin membrane can be attributed to the incomplete addition of quaternary ammonium functionalities to the PVDF polymer during membrane manufacturing [34]. Upon fouling, these peaks are shifted due to electrostatic and hydrophobic interactions between the membrane and the foulant. Strength of the $\nu_{(+N-C)}$ was affected by the degree of electrostatic interactions; thus, a higher red shift of $\Delta\nu\ 7.3\text{ cm}^{-1}$ was observed for HA fouled membranes compared to the red shift of $\Delta\nu\ 2.2\text{ cm}^{-1}$ for HA-Ca²⁺, which signifies the reduced negative charge density on HA-Ca²⁺. The $\nu_{(C=C)}$ provides insight into the hydrophobic π - π donor-acceptor interactions as well as cation- π interactions. Broad and blue shifted peak at $\Delta\nu\ 2.3\text{ cm}^{-1}$ for $\nu_{(C=C)}$ of HA-Ca²⁺ indicate the accumulation of HS via cation- π bridging interactions (**Fig. 6**). Therefore, enhanced fouling by membrane-HA-Ca²⁺ ternary complexes can be observed in ATR-FTIR data. This notion supported the accumulation of foulants on the membrane surface via foulant-foulant interactions. In contrast, the HA fouled membranes showed a red shift of $\Delta\nu\ 4.3\text{ cm}^{-1}$ for $\nu_{(C=C)}$ due to membrane C=C bond weakening upon electrons acceptance from π -donors of the HA.

CH₂ and CH₃ deformations (~1515-1145 cm⁻¹): Dispersive forces among the membrane and the foulant have caused blue shifts for the deformation band corresponding to CH₂ in-plane bending or scissoring (1335.9 cm^{-1} by $\Delta\nu\ 0.5\text{ cm}^{-1}$ for HA, by $\Delta\nu\ 1.8\text{ cm}^{-1}$ for HA-Ca²⁺) (**Fig. 4 (b)**). Higher blue shift recognized for the HA-Ca²⁺ fouled membranes confirmed significant CH-donor-acceptor hydrophobic interactions between the membrane and the foulant. Red shifts observed for C-H deformations of H-C-N⁺ supported the electrostatic interactions described previously (**Fig. 4 (b)**).

C-C stretching vibrations and C-C-C skeletal vibrations (~1090-900 cm⁻¹): The intensification of the C-C stretching vibrations ($\nu_{(C-C)}$) at 1072.4 and 1056.3 cm^{-1} and the C-C-C skeletal vibration ($\nu_{(C-C-C)}$) band (596 cm^{-1}) observed after fouling is due to the HA accumulation on the membrane surface. Further, the de-convoluted peaks for $\nu_{(C-C)}$ showed blue shifts after HA, and HA-Ca²⁺ fouling and the shifts are illustrated in **Fig. 4 (f), (g), and (h)**. The shifts are due to the London dispersive van der Waals interactions between the polymeric membrane backbone and the foulant. Moreover, there was no significant effect of Ca²⁺ on these interactions as there were no marked changes to the transmittance peaks between membrane-HA and membrane-HA-Ca²⁺ complexes.

Foulant structural features: The appearance of new bands after membrane fouling can be ascribed to foulant features. One such feature is the C-O stretch of carboxyl groups ($\nu_{(C-O)}$)

COOH) at 1121.2 cm^{-1} for the HA-Ca²⁺ and at 1120.9 cm^{-1} for the HA as shown in **Fig. 4 (f)** and **(g)**, respectively. A noticeable high frequency for $\nu_{(\text{C-O})\text{COOH}}$ of HA-Ca²⁺ is due to the strengthening of the C–O bond due to inner-sphere Ca²⁺ coordination as shown in **Fig. 6** [7, 41-43]. Further, the Ca²⁺ complexation to HA was supported by the shift obtained for COO⁻ stretching vibrations ($\nu_{(\text{COO}^-)}$). The $\nu_{(\text{COO}^-)}$ band observed for HA-Ca²⁺ was blue shifted by $\Delta\nu$ 10.0 cm^{-1} compared to HA fouled membrane (**Fig. 4 (c) and (d)**). The appearance of a C=O stretching band of carboxyl groups ($\nu_{(\text{C=O})\text{COOH}}$) at 1726.1 cm^{-1} for the HA-Ca²⁺ and at 1724.0 cm^{-1} for the HA is identified as a foulant feature and shown in the supporting documentation (**Fig. S.4**) [40, 47]. The aromatic C=C stretching in the $1658\text{-}1647\text{ cm}^{-1}$ [49] region was also identified as a new feature to the spectrum, which further confirmed the presence of HS on the AEM surface.

3.4 Postulated mechanism of membrane fouling by HA and HA-Ca²⁺

Fig. 6

Based on the results presently shown and in corroboration with published data [11-13, 24, 46-49], a plausible mechanism for membrane fouling by HA and HA-Ca²⁺ is proposed (**Fig. 6**). Literature data show the formation of Ca²⁺ and dissolved organic carbon complexes, namely HA-Ca²⁺ and FA-Ca²⁺ at typical groundwater pH conditions (6.36-9.87) [15, 25, 26, 48-52]. This study specifically focused on the effect of incorporating Ca²⁺ into HA and observed physiochemical changes that occurred when HA-Ca²⁺ complexes participated as the foulant for EDR-AEMs. Our vibrational spectroscopic data confirmed the electrostatic double-layer interactions of HA or HA-Ca²⁺ with the AEM surface. **Fig. 6** illustrates the formation of the electrostatic double-layer interactions. Further, possible hydrophobic interactions with non-polar aliphatic and aromatic portions within the macromolecular structure of HA and polymeric backbone structure of the membrane surface were also considered when postulating the mechanism.

As shown in **Fig. 6**, part of the HS's negative charge is reduced due to inner-sphere Ca²⁺ complexation with COO⁻ sites. This fact predominantly affects the formation of membrane-HA-Ca²⁺ ternary complexes. Further free Ca²⁺ present in the synthetic waters forms inter-molecular bridges and cation- π complexes (**Fig. 6**) to facilitate HA accumulation. Therefore, free Ca²⁺ has enhanced the stability of the HA derived foulants on AEM benign to EDR self-cleaning cycle. The HA derived mechanism of fouling deviates significantly in the presence of Ca²⁺ in water [10]. The irreversible nature of hydrophobic interactions (i.e., CH- π , cation-

π , π - π , and dispersive interactions) between HA-Ca²⁺ and the membrane compared to HA was observed by IR data after the SDS treatment. Common membrane-foulant interactions irrespective of the presence or absence of Ca²⁺ were identified as hydrogen-bonding between membrane-bound water and the HS, CH- π interactions between CH₂ of the membrane and π -acceptors, van der Waals interactions between the hydrocarbon skeleton and the HS, polar- π interactions among the quaternary ammonium sites and π -donors, and salt bridges due to ionic interactions between quaternary ammonium sites and negative functional groups like carboxylate in HS.

4. Conclusions

HA or HA-Ca²⁺ interacts differently with AEM surfaces leading to partial or totally irreversible membrane fouling. Electrostatic interactions partially account for reversible components of HA and HA-Ca²⁺ fouled membranes, whereas HA-Ca²⁺ showed irreversible fouling due to inter-molecular bridging interactions. Although NaCl or SDS removes outermost surface-bound organic moieties from the membranes, a total recovery of the membrane functionality was not possible. SDS desorption allowed demarcation of hydrophobic interactions in the formation of membrane-foulant complexes. HA-Ca²⁺ foulants accumulated via cation- π interactions were mainly desorbed with SDS. SEM and IR data from the sequential desorption study further suggested the comparatively high irreversible nature of the HA-Ca²⁺ fouling compared to the HA fouling. Overall, the results indicated the requirement of an alternative method for the self-cleaning process in the EDR systems to combat irreversible fouling that occurs by organometallic complexes.

5. Acknowledgements

We acknowledge the financial support from the Joint Research Program of the National Science Foundation of Sri Lanka (ICRP/NSF-NSFC/2019/BS/03) and the National Natural Science Foundation of China (21861142020). Also, we appreciate the education and research program of the China-Sri Lanka Joint Research and Demonstration Center for Water Technology by the Chinese Academy of Sciences. Further, we acknowledge to China-Sri Lanka Research Grant Project under the Ministry of Water Supply, Sri Lanka.

6. References

1. Thurman, E. M. *Organic Geochemistry of Natural Waters. Organic Geochemistry of Natural Waters* (1985). doi:10.1007/978-94-009-5095-5.
2. Connell, D. W. *Basic Concepts of Environmental Chemistry. Basic Concepts of Environmental Chemistry* (2005). doi:10.1201/b12378.
3. Loffredo, E. & Senesi, N. The role of humic substances in the fate of anthropogenic organic pollutants in soil with emphasis on endocrine disruptor compounds. in *Soil and Water Pollution Monitoring, Protection and Remediation* (2007). doi:10.1007/978-1-4020-4728-2_4.
4. Philippe, A. & Schaumann, G. E. Interactions of dissolved organic matter with natural and engineered inorganic colloids: A review. *Environmental Science and Technology* (2014) doi:10.1021/es502342r.
5. Piccolo, A. The supramolecular structure of humic substances. *Soil Science* (2001) doi:10.1097/00010694-200111000-00007.
6. Samios, S., Lekkas, T., Nikolaou, A. & Golfinopoulos, S. Structural investigations of aquatic humic substances from different watersheds. *Desalination* (2007) doi:10.1016/j.desal.2006.05.038.
7. Adusei-Gyamfi, J., Ouddane, B., Rietveld, L., Cornard, J. P. & Criquet, J. Natural organic matter-cations complexation and its impact on water treatment: A critical review. *Water Research* (2019) doi:10.1016/j.watres.2019.05.064.
8. Matilainen, A., Vepsäläinen, M. & Sillanpää, M. Natural organic matter removal by coagulation during drinking water treatment: A review. *Adv. Colloid Interface Sci.* **159**, 189–197 (2010).
9. Tian, J., Ernst, M., Cui, F. & Jekel, M. Effect of different cations on UF membrane fouling by NOM fractions. *Chem. Eng. J.* **223**, 547–555 (2013).
10. Hansima, M. A. C. K. *et al.* Fouling of Ion Exchange Membranes used in the Electrodialysis Reversal Advanced Water Treatment: A Review. *Chemosphere* 127951 (2020) doi:10.1016/j.chemosphere.2020.127951.
11. Persico, M. *et al.* Formation of peptide layers and adsorption mechanisms on a negatively charged cation-exchange membrane. *J. Colloid Interface Sci.* (2017) doi:10.1016/j.jcis.2017.08.029.
12. Shi, L. *et al.* Nutrient recovery from pig manure digestate using electrodialysis reversal: Membrane fouling and feasibility of long-term operation. *J. Memb. Sci.* (2019) doi:10.1016/j.memsci.2018.12.037.
13. Xu, H. *et al.* Outlining the Roles of Membrane-Foulant and Foulant-Foulant Interactions in Organic Fouling During Microfiltration and Ultrafiltration: A Mini-Review. *Frontiers in Chemistry* (2020) doi:10.3389/fchem.2020.00417.
14. Bacher, L. E. *et al.* Coupling coagulation using tannin-based product with electrodialysis reversal to water treatment: A case study. *J. Environ. Chem. Eng.* (2017) doi:10.1016/j.jece.2017.11.002.
15. James Watkins, E. & Pfromm, P. H. Capacitance spectroscopy to characterize organic fouling of electrodialysis membranes. *J. Memb. Sci.* (1999) doi:10.1016/S0376-7388(99)00144-1.
16. Lindstrand, V., Sundström, G. & Jönsson, A. S. Fouling of electrodialysis membranes by organic substances. *Desalination* (2000) doi:10.1016/S0011-9164(00)00026-6.

17. Ang, W. S. & Elimelech, M. Protein (BSA) fouling of reverse osmosis membranes: Implications for wastewater reclamation. *J. Memb. Sci.* (2007) doi:10.1016/j.memsci.2007.03.018.
18. Persico, M. *et al.* Prevention of peptide fouling on ion-exchange membranes during electro dialysis in overlimiting conditions. *J. Memb. Sci.* (2017) doi:10.1016/j.memsci.2017.08.039.
19. Sanchez-Camazano, M., Sanchez-Martin, M. J. & Rodriguez-Cruz, M. S. Sodium dodecyl sulphate-enhanced desorption of atrazine: Effect of surfactant concentration and of organic matter content of soils. *Chemosphere* (2000) doi:10.1016/S0045-6535(99)00503-2.
20. Makehelwala, M., Wei, Y., Weragoda, S. K. & Weerasooriya, R. Ca²⁺ and SO₄²⁻ interactions with dissolved organic matter: Implications of groundwater quality for CKDu incidence in Sri Lanka. *J. Environ. Sci. (China)* (2020) doi:10.1016/j.jes.2019.09.018.
21. Wang, Y., Zhang, Z., Jiang, C. & Xu, T. Electrodialysis process for the recycling and concentrating of tetramethylammonium hydroxide (TMAH) from photoresist developer wastewater. *Ind. Eng. Chem. Res.* (2013) doi:10.1021/ie4023995.
22. Zhou, J. *et al.* Application of electro dialysis to extract 5'-ribonucleotides from hydrolysate: Efficient decolorization and membrane fouling. *RSC Adv.* (2018) doi:10.1039/c8ra02550a.
23. Pearson, T. W., Dawson, H. J. & Lackey, H. B. Natural Occurring Levels of Dimethyl Sulfoxide in Selected Fruits, Vegetables, Grains, and Beverages. *J. Agric. Food Chem.* (1981) doi:10.1021/jf00107a049.
24. Strathmann, H. *Ion-Exchange Membrane Separation Processes. Membrane Science and Technology Series, 9* (2004).
25. Park, J. S., Song, J. H., Yeon, K. H. & Moon, S. H. Removal of hardness ions from tap water using electromembrane processes. *Desalination* (2007) doi:10.1016/j.desal.2005.12.031.
26. Lemay, N., Mikhaylin, S. & Bazinet, L. Voltage spike and electroconvective vortices generation during electro dialysis under pulsed electric field: Impact on demineralization process efficiency and energy consumption. *Innov. Food Sci. Emerg. Technol.* (2019) doi:10.1016/j.ifset.2018.12.004.
27. Todeschini, S. *et al.* Assessment of the performance of electro dialysis in the removal of the most potent odor-active compounds of herring milt hydrolysate: Focus on ion-exchange membrane fouling and water dissociation as limiting process conditions. *Membranes (Basel)*. (2020) doi:10.3390/membranes10060127.
28. Huang, C., Xu, T., Zhang, Y., Xue, Y. & Chen, G. Application of electro dialysis to the production of organic acids: State-of-the-art and recent developments. *Journal of Membrane Science* (2007) doi:10.1016/j.memsci.2006.11.026.
29. Lee, H. J., Choi, J. H., Cho, J. & Moon, S. H. Characterization of anion exchange membranes fouled with humate during electro dialysis. *J. Memb. Sci.* (2002) doi:10.1016/S0376-7388(01)00792-X.
30. Hakim, A., Suzuki, T. & Kobayashi, M. Strength of Humic Acid Aggregates: Effects of Divalent Cations and Solution pH. *ACS Omega* (2019) doi:10.1021/acsomega.9b00124.
31. Wang, T. H., Yen, Y. J., Hsieh, Y. K. & Wang, J. Size effect of calcium-humic acid non-rigid complexes on the fouling behaviors in nanofiltration: An LA-ICP-MS study. *Colloids Surfaces A Physicochem. Eng. Asp.* (2017) doi:10.1016/j.colsurfa.2016.10.062.
32. Xu, F. *et al.* Specific ion effects on the aggregation behavior of aquatic natural organic matter. *J. Colloid Interface Sci.* (2019) doi:10.1016/j.jcis.2019.09.001.

33. Iskrenova-Tchoukova, E., Kalinichev, A. G. & Kirkpatrick, R. J. Metal Cation Complexation with Natural Organic Matter in Aqueous Solutions: Molecular Dynamics Simulations and Potentials of Mean Force. *Langmuir* **26**, 15909–15919 (2010).
34. Wang, J. *et al.* Enhanced gypsum scaling by organic fouling layer on nanofiltration membrane: Characteristics and mechanisms. *Water Res.* (2016) doi:10.1016/j.watres.2016.01.019.
35. Golubenko, D. V., Shaydullin, R. R. & Yaroslavl'tsev, A. B. Improving the conductivity and permselectivity of ion-exchange membranes by introduction of inorganic oxide nanoparticles: impact of acid–base properties. *Colloid Polym. Sci.* (2019) doi:10.1007/s00396-019-04499-1.
36. Tan, L. *et al.* Coagulation behavior of humic acid in aqueous solutions containing Cs⁺, Sr²⁺ and Eu³⁺: DLS, EEM and MD simulations. *Environ. Pollut.* (2018) doi:10.1016/j.envpol.2018.02.019.
37. Allison, R. P. Electrodialysis reversal in water reuse applications. *Desalination* (1995) doi:10.1016/0011-9164(95)00082-8.
38. Zhao, Z., Shi, S., Cao, H., Shan, B. & Sheng, Y. Property characterization and mechanism analysis on organic fouling of structurally different anion exchange membranes in electrodialysis. *Desalination* (2018) doi:10.1016/j.desal.2017.11.021.
39. Zhao, Z., Shi, S., Cao, H., Li, Y. & Van der Bruggen, B. Comparative studies on fouling of homogeneous anion exchange membranes by different structured organics in electrodialysis. *J. Environ. Sci. (China)* (2019) doi:10.1016/j.jes.2018.07.018.
40. Jialin, L., Yazhen, W., Changying, Y., Guangdou, L. & Hong, S. Membrane catalytic deprotonation effects. *J. Memb. Sci.* (1998) doi:10.1016/S0376-7388(98)00126-4.
41. Bdiri, M. *et al.* Identification of phenolic compounds and their fouling mechanisms in ion-exchange membranes used at an industrial scale for wine tartaric stabilization by electrodialysis. *Sep. Purif. Technol.* (2020) doi:10.1016/j.seppur.2019.115995.
42. Langevin, M. E. & Bazinet, L. Ion-exchange membrane fouling by peptides: A phenomenon governed by electrostatic interactions. *J. Memb. Sci.* (2011) doi:10.1016/j.memsci.2010.12.031.
43. Su, Z., Cocinero, E. J., Stanca-Kaposta, E. C., Davis, B. G. & Simons, J. P. Carbohydrate-aromatic interactions: A computational and IR spectroscopic investigation of the complex, methyl α -l-fucopyranoside \cdot toluene, isolated in the gas phase. *Chem. Phys. Lett.* (2009) doi:10.1016/j.cplett.2009.02.043.
44. Monvisade, P. & Siriphannon, P. Chitosan intercalated montmorillonite: Preparation, characterization and cationic dye adsorption. *Appl. Clay Sci.* (2009) doi:10.1016/j.clay.2008.04.013.
45. Liu, X., Wazne, M., Chou, T., Xiao, R. & Xu, S. Influence of Ca²⁺ and Suwannee River Humic Acid on aggregation of silicon nanoparticles in aqueous media. *Water Res.* (2011) doi:10.1016/j.watres.2010.08.022.
46. Viana, R. B., Da Silva, A. B. F. & Pimentel, A. S. Infrared spectroscopy of anionic, cationic, and zwitterionic surfactants. *Adv. Phys. Chem.* (2012) doi:10.1155/2012/903272.
47. Dong, H. & Lo, I. M. C. Influence of calcium ions on the colloidal stability of surface-modified nano zero-valent iron in the absence or presence of humic acid. *Water Res.* (2013) doi:10.1016/j.watres.2013.02.022.
48. Lee, H. J., Hong, M. K., Han, S. D., Cho, S. H. & Moon, S. H. Fouling of an anion exchange membrane in the electrodialysis desalination process in the presence of organic foulants. *Desalination* (2009) doi:10.1016/j.desal.2008.01.036.

49. Garcia-Vasquez, W. *et al.* Evolution of anion-exchange membrane properties in a full scale electro dialysis stack. *J. Memb. Sci.* (2013) doi:10.1016/j.memsci.2013.06.042.
50. Korngold, E., de Körösy, F., Rahav, R. & Taboch, M. F. Fouling of anionselective membranes in electro dialysis. *Desalination* (1970) doi:10.1016/S0011-9164(00)80230-1.
51. Lee, H. J. & Moon, S. H. Enhancement of electro dialysis performances using pulsing electric fields during extended period operation. *J. Colloid Interface Sci.* (2005) doi:10.1016/j.jcis.2005.02.027.
52. Makehelwala, M., Wei, Y., Weragoda, S. K., Weerasooriya, R. & Zheng, L. Characterization of dissolved organic carbon in shallow groundwater of chronic kidney disease affected regions in Sri Lanka. *Sci. Total Environ.* (2019) doi:10.1016/j.scitotenv.2018.12.435.

7. List of figures

Fig. 1: Conductivity (mS cm^{-1}) vs fouling period (min) plot of feed solutions containing (a) Sigma-Aldrich humic acid ($\sim 2 \text{ mg L}^{-1}$, TOC), 0.001 M NaCl and 0.001 M NaHCO_3 at pH ~ 8 (HA) and (b) Sigma-Aldrich humic acid ($\sim 2 \text{ mg L}^{-1}$, TOC), 0.001 M NaCl, 0.001 M NaHCO_3 and $\text{CaCl}_2 \cdot 2\text{H}_2\text{O}$ ($\sim 200 \text{ mg L}^{-1}$, Ca^{2+}) at pH ~ 8 (HA- Ca^{2+})

Fig. 2: Variation of desalination (D%), decolourisation (A%) and removal of DOC and/or Ca^{2+} ($R_{\text{DOC}}\%$)/($R_{\text{Ca}^{2+}}\%$) as a function of feed solution cycles in the presence of HA ($\sim 2 \text{ mg L}^{-1}$, TOC, 0.001 M NaCl and 0.001 M NaHCO_3 at pH ~ 8) or HA- Ca^{2+} ($\sim 2 \text{ mg L}^{-1}$, TOC, 0.001 M NaCl, 0.001 M NaHCO_3 and $\sim 200 \text{ mg L}^{-1}$, Ca^{2+} at pH ~ 8)

Fig. 3: High-resolution SEM images illustrating surface morphology of (a) activated AEM after immersing the virgin membrane in 0.001 M NaCl for 24 hours, (b) AEM fouled by HA and (c) AEM fouled by HA- Ca^{2+} . Aggregated HA- Ca^{2+} foulants on/in AEM pores are labeled, (d) 2% (w/w) NaCl desorbed, HA fouled membrane and (e) 2% (w/w) NaCl desorbed, HA- Ca^{2+} fouled membrane, (f) 0.03% (w/w) SDS desorbed, HA fouled membrane and (g) 0.03% (w/w) SDS desorbed, HA- Ca^{2+} fouled membrane. **Label A** presents recovered AEM pores by desorption and **label B** shows the remaining foulant after desorption

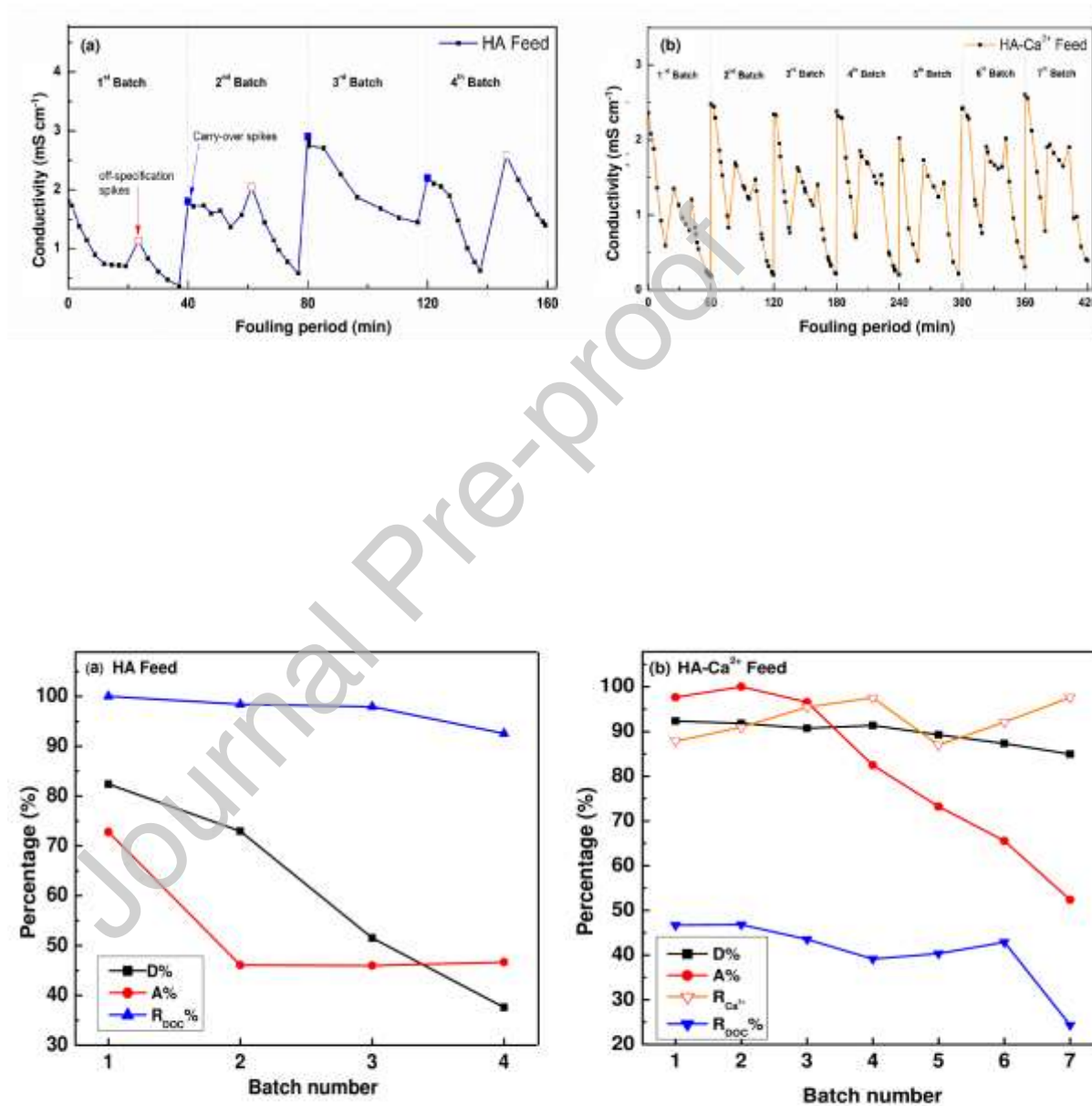
Fig. 4: FTIR-ATR spectra of virgin, HA fouled and HA- Ca^{2+} fouled CJMA-4 AEMs at (a) high frequency (ν , $4000\text{-}2500 \text{ cm}^{-1}$) and (b) low frequency (ν , $1800\text{-}400 \text{ cm}^{-1}$) spectral regions with O-H stretching (ν , $3670\text{-}3070 \text{ cm}^{-1}$), C-H stretching (ν , $3070\text{-}2800 \text{ cm}^{-1}$), C=C stretching (ν , $1750\text{-}1550 \text{ cm}^{-1}$), CH_2 and CH_3 deformations (ν , $1515\text{-}1145 \text{ cm}^{-1}$), C-C stretching (ν , $1090\text{-}900 \text{ cm}^{-1}$) and CH_2 bending (ν , $>800 \text{ cm}^{-1}$) vibrations to illustrate peak shifts due to membrane-foulant interactions. (c-e) Deconvoluted spectral regions illustrating foulant features of HA- Ca^{2+} , HA fouled membranes and virgin membrane for the range $1720\text{-}1660 \text{ cm}^{-1}$. (f-h) Deconvoluted spectral regions illustrating foulant features of HA- Ca^{2+} , HA fouled membranes and virgin membrane for the range $1140\text{-}1040 \text{ cm}^{-1}$.

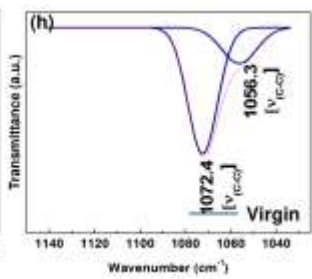
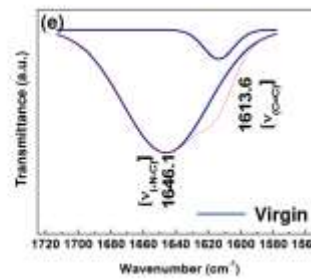
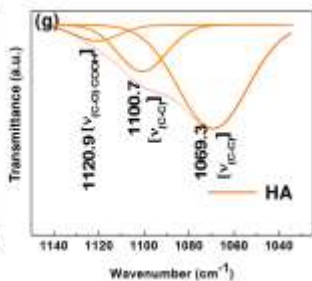
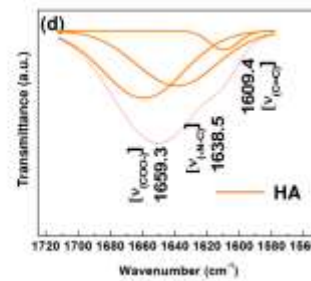
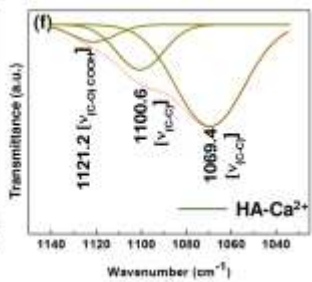
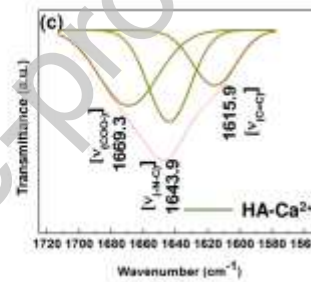
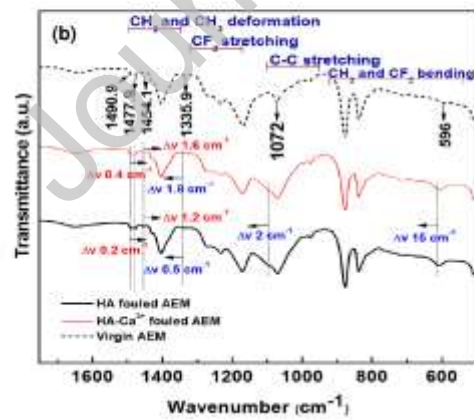
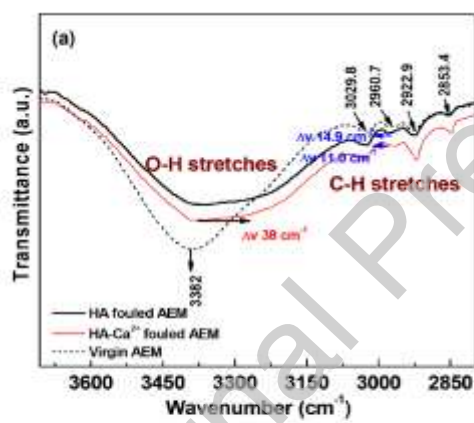
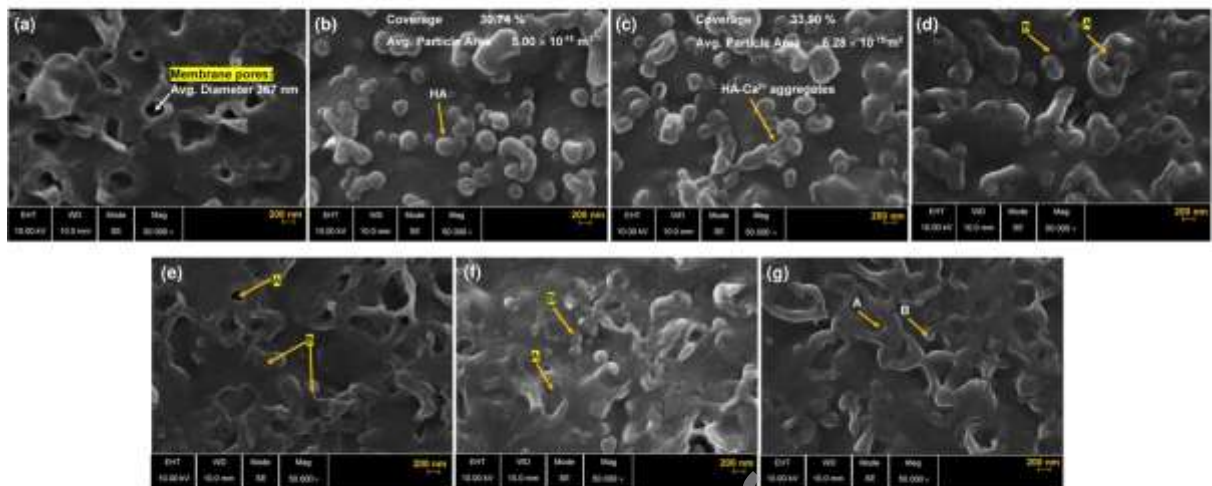
Fig. 5: ATR-FTIR spectra of 2% (w/w) NaCl and 0.03% (w/w) SDS desorbed fouled membranes. (a) High (ν , $4000\text{-}2500 \text{ cm}^{-1}$), (b) mid (ν , $1800\text{-}1300 \text{ cm}^{-1}$) and (c) low (ν , $1400\text{-}500 \text{ cm}^{-1}$) frequency spectral regions of HA- Ca^{2+} fouled membranes. (d) High (ν , $4000\text{-}2500 \text{ cm}^{-1}$), (e) mid (ν , $1800\text{-}1300 \text{ cm}^{-1}$) and (f) low (ν , $1400\text{-}500 \text{ cm}^{-1}$) frequency spectral regions of HA fouled membranes

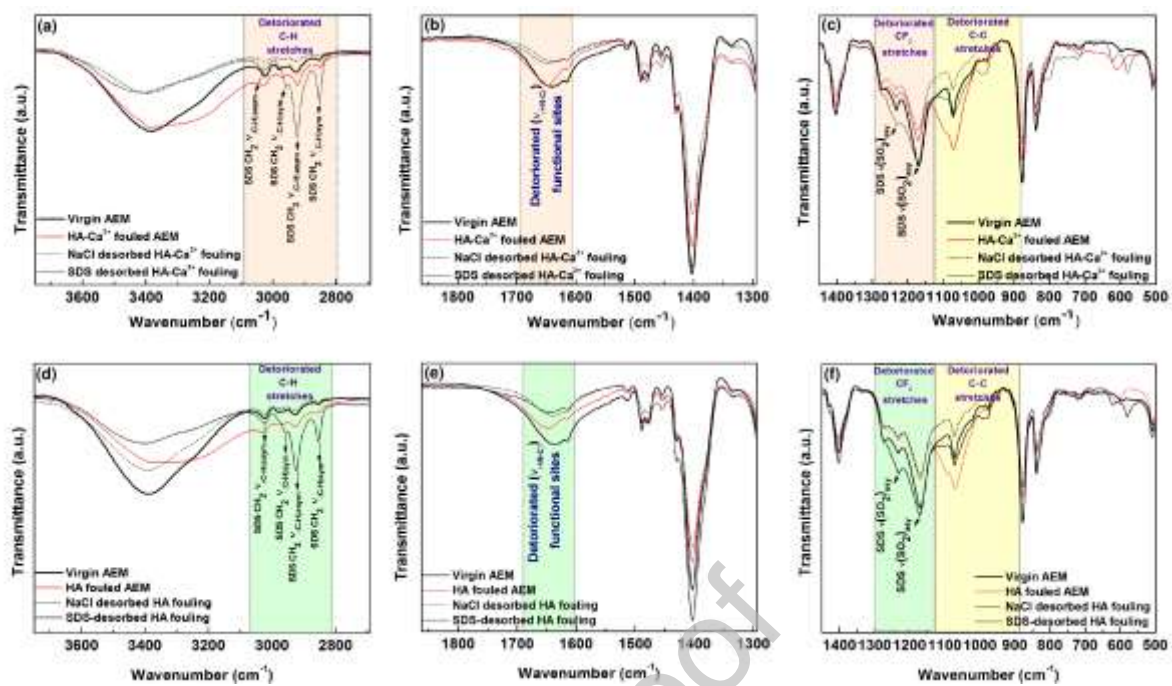
Fig. 6: Schematic illustration of the interactions involved in membrane-HA complexes with and without calcium ions, elucidated by the vibrational spectroscopic data

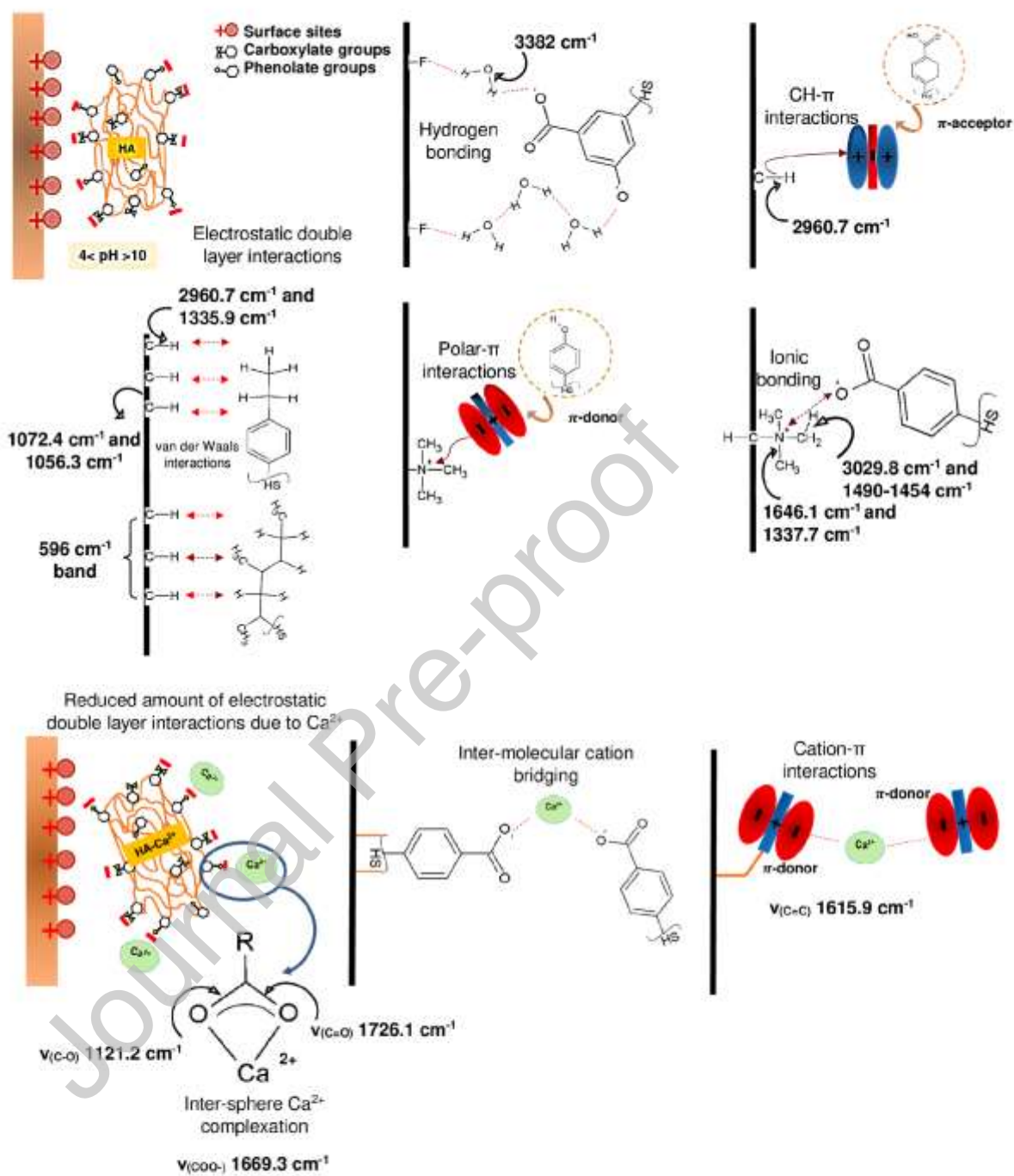
8. List of tables

Table 1: Solution properties of 2% (w/w) NaCl and 0.03% (w/w) SDS desorption solutions at RT before and after the equilibration with fouled AEMs









Declaration of interests

The authors declare that they have no known competing financial interests or personal relationships that could have appeared to influence the work reported in this paper.

The authors declare the following financial interests/personal relationships which may be considered as potential competing interests:

Journal Pre-proof